

## ***Supplementary Information***

### **Thermally induced nanostructuring for the synthesis of core/shell-structured CoO/CoS<sub>x</sub> electrocatalyst**

Min Soo Kim<sup>a†</sup>, Muhammad Awais Abbas<sup>b†</sup>, Raju Thota<sup>b†</sup> and Jin Ho Bang\*<sup>abc</sup>

<sup>a</sup>*Department of Bionano Technology, Hanyang University, 55 Hanyangdaehak-ro, Sangnok-gu, Ansan,  
Gyeonggi-do 15588, Republic of Korea*

<sup>b</sup>*Nanosensor Research Institute, Hanyang University, 55 Hanyangdaehak-ro, Sangnok-gu, Ansan,  
Gyeonggi-do 15588, Republic of Korea*

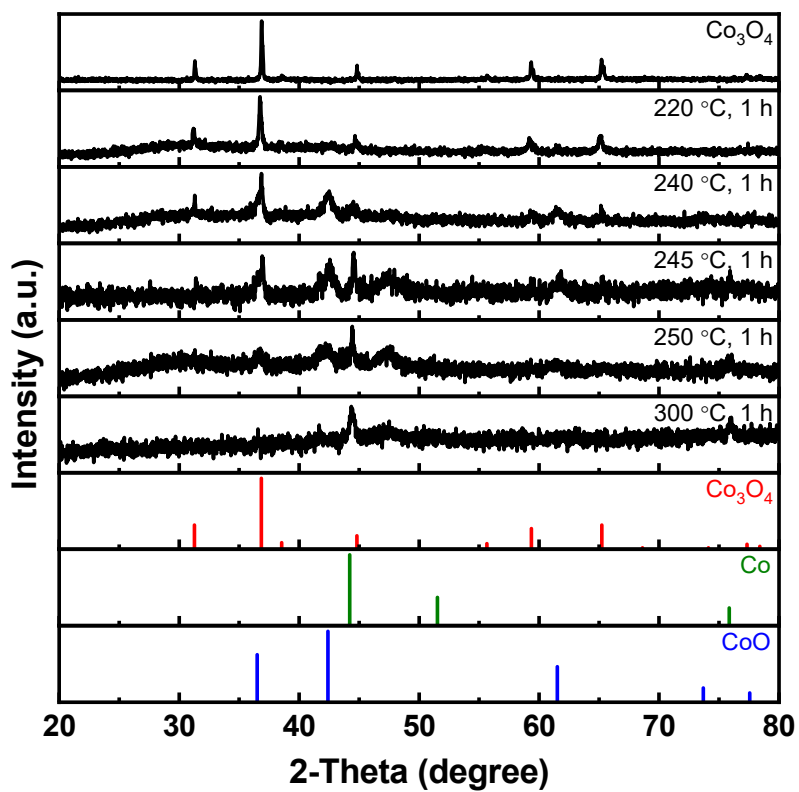
<sup>c</sup>*Department of Chemical and Molecular Engineering, Hanyang University, 55 Hanyangdaehak-ro,  
Sangnok-gu, Ansan, Gyeonggi-do 15588, Republic of Korea*

#### **Author Contributions:**

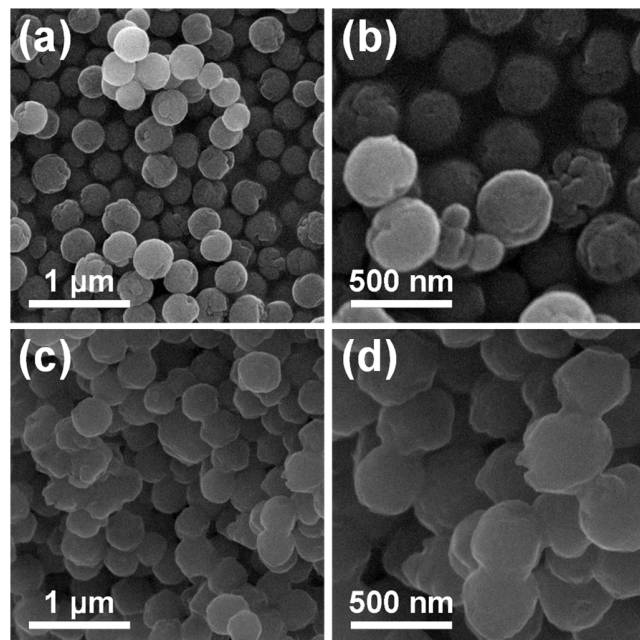
<sup>†</sup>These authors contributed equally to this work.

\*Corresponding Author

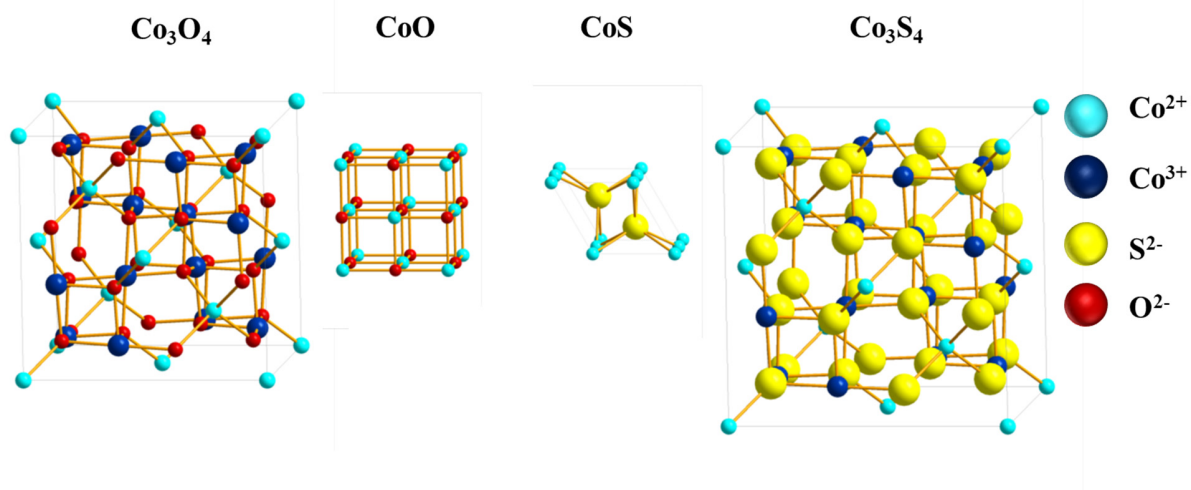
E-mail: jbang@hanyang.ac.kr



**Fig. S1** XRD patterns of intermediates obtained during a hot H<sub>2</sub> treatment of Co<sub>3</sub>O<sub>4</sub> at various temperatures for 1 h.

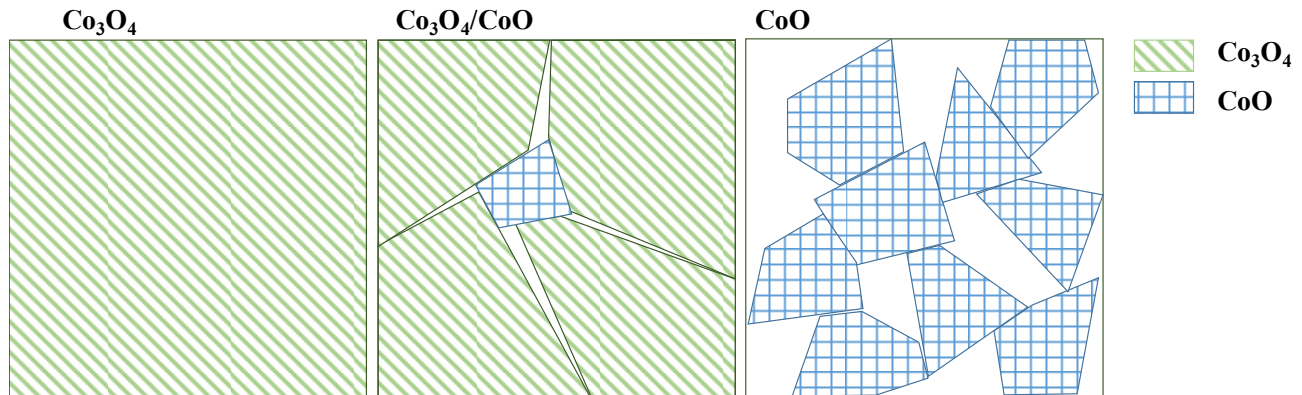


**Fig. S2** SEM images of Co<sub>3</sub>O<sub>4</sub> (a,b) before and (c,d) after a hot H<sub>2</sub> treatment at 300 °C for 1 h.



**Fig. S3** The crystal structure of cobalt oxides and cobalt sulfides.

**Scheme S1** Schematic representation of the grain fracture of  $\text{Co}_3\text{O}_4$  and the formation of mesoporous  $\text{CoO}$  with smaller crystallites from bulk  $\text{Co}_3\text{O}_4$  under a reducing environment of hot  $\text{NH}_3$ .



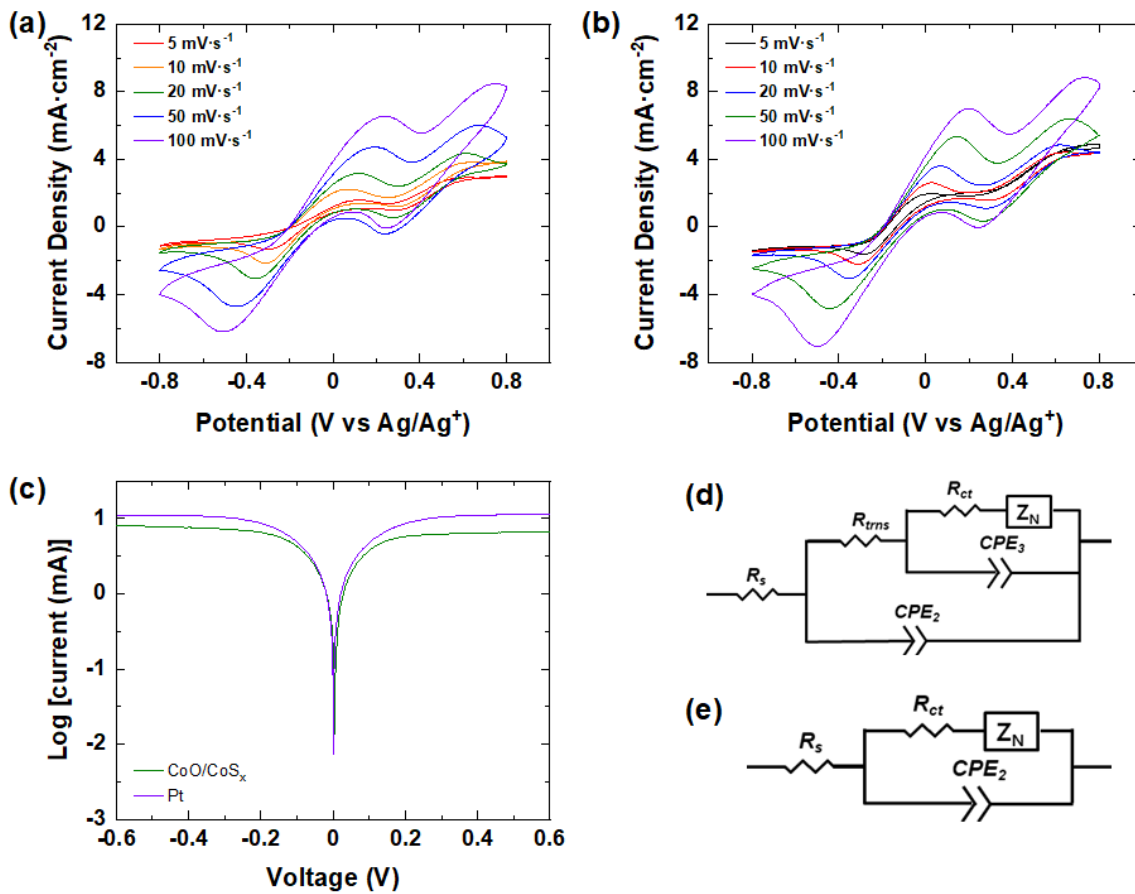


**Fig. S4** Cyclic voltammograms of (a) CoO/CoS<sub>x</sub> and (b) Pt electrodes at various scan rates. (c) Tafel polarization curves of CoO/CoS<sub>x</sub> and Pt counter electrodes. Equivalent circuits used for fitting the Nyquist plots of (d) CoO/CoS<sub>x</sub> and (e) Pt counter electrodes.  $R_s$  is the equivalent series resistance,  $R_{ct}$  is the charge transfer resistance,  $Z_N$  is the Nernst diffusion impedance,  $R_{trns}$  is the electron transport resistance in the carbon layer, and  $CPE_2$  and  $CPE_3$  are the constant phase elements associated with resistances.

**Table S1** Various resistance values extracted from fitting the Nyquist plots of CoO/CoS<sub>x</sub> and Pt electrodes. EIS was carried out with symmetric dummy cells.

Counter Electrode	$R_s$ ( $\Omega \cdot \text{cm}^2$ )	$R_{trns}$ ( $\Omega \cdot \text{cm}^2$ )	$R_{ct}$ ( $\Omega \cdot \text{cm}^2$ )	$Z_N$ ( $\Omega \cdot \text{cm}^2$ )
CoO/CoS <sub>x</sub>	3.30	0.57	0.91	1.35
Pt	3.31	-	0.97	1.32

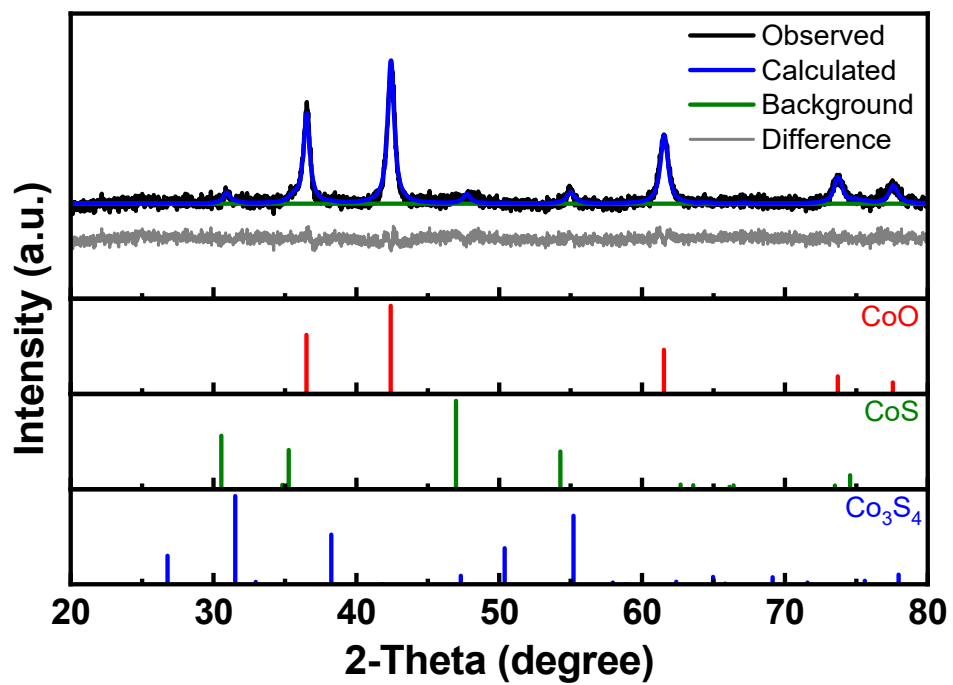


**Fig. S5** XRD pattern of  $\text{CoO}/\text{CoS}_x$  and Rietveld refinement result that determines the composition of each component ( $\text{CoO}$ : 86.2%,  $\text{CoS}$ : 11.9%, and  $\text{Co}_3\text{S}_4$ : 1.9%).

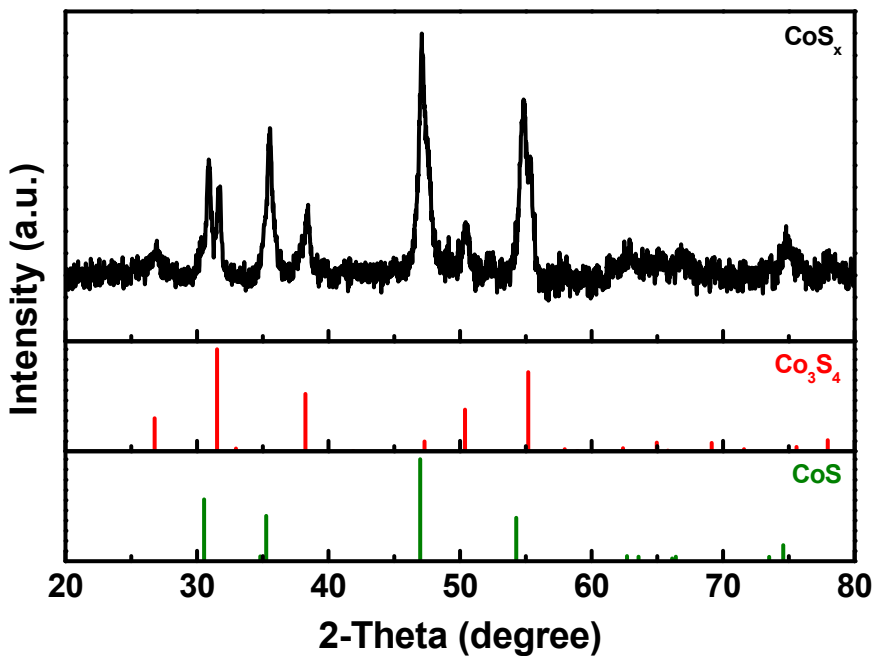


**Fig. S6** XRD pattern of  $\text{CoS}_x$  obtained at 300 °C for 1 h. The compositional percentages of CoS and  $\text{Co}_3\text{S}_4$  determined by Rietveld refinement were 76.5 and 23.5%, respectively.

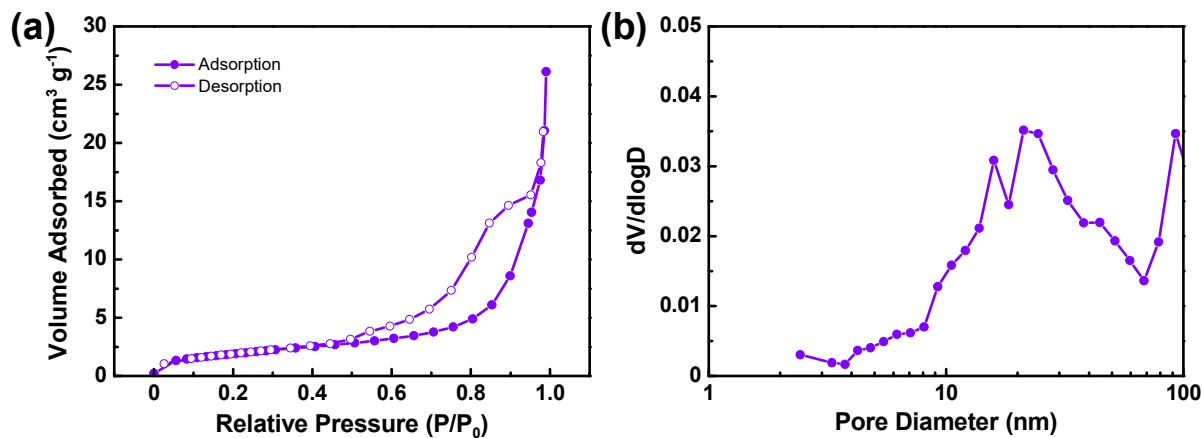


**Fig. S7** (a)  $\text{N}_2$  physisorption isotherms and (b) pore size distributions of  $\text{CoS}_x$ . The BET surface area was  $7.34 \text{ m}^2 \cdot \text{g}^{-1}$  and the total pore volume was  $0.047 \text{ cm}^3 \cdot \text{g}^{-1}$ .

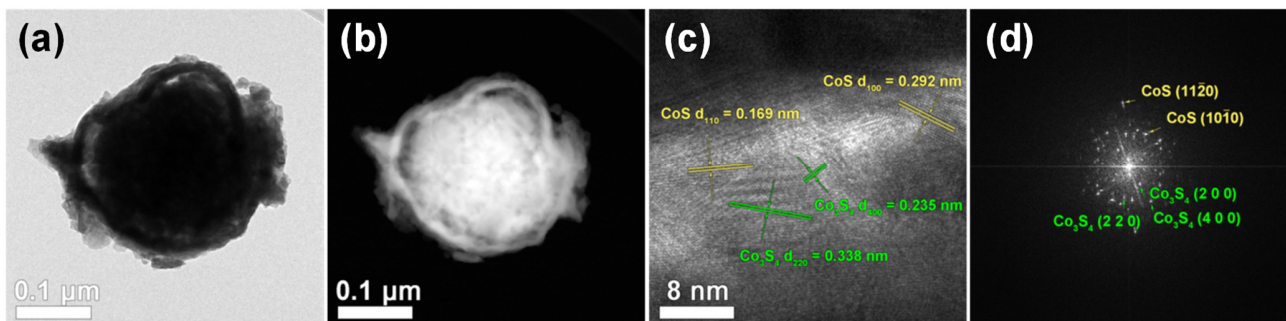


**Fig. S8** (a-c) TEM images and (d) FFT patterns of  $\text{CoS}_x$ .

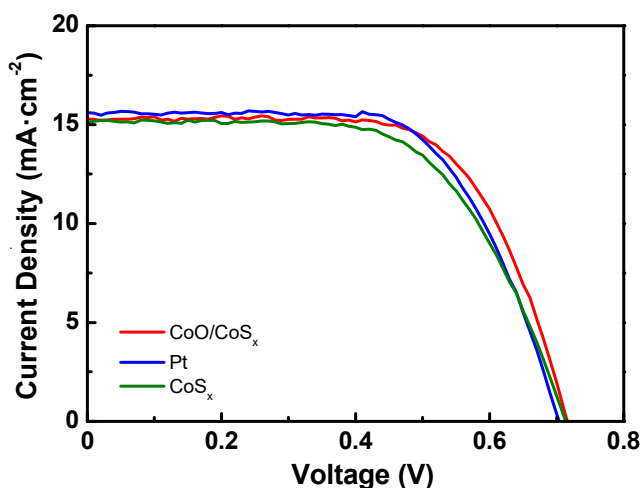


**Fig. S9**  $J-V$  curve of DSSCs assembled with various CEs made of CoO/CoS<sub>x</sub>, Pt, and CoS<sub>x</sub>.

**Table S2**  $J-V$  parameters of DSSCs fabricated with the above CEs.

CE	$J_{sc}$ (mA·cm <sup>2</sup> )	$V_{oc}$ (V)	FF	PCE (%)
CoO/CoS <sub>x</sub>	$15.5 \pm 0.3$	$0.73 \pm 0.01$	$0.66 \pm 0.02$	$7.27 \pm 0.06$
Pt	$15.9 \pm 0.2$	$0.70 \pm 0.01$	$0.65 \pm 0.01$	$7.12 \pm 0.05$
CoS <sub>x</sub>	$15.1 \pm 0.5$	$0.71 \pm 0.02$	$0.62 \pm 0.03$	$6.73 \pm 0.16$

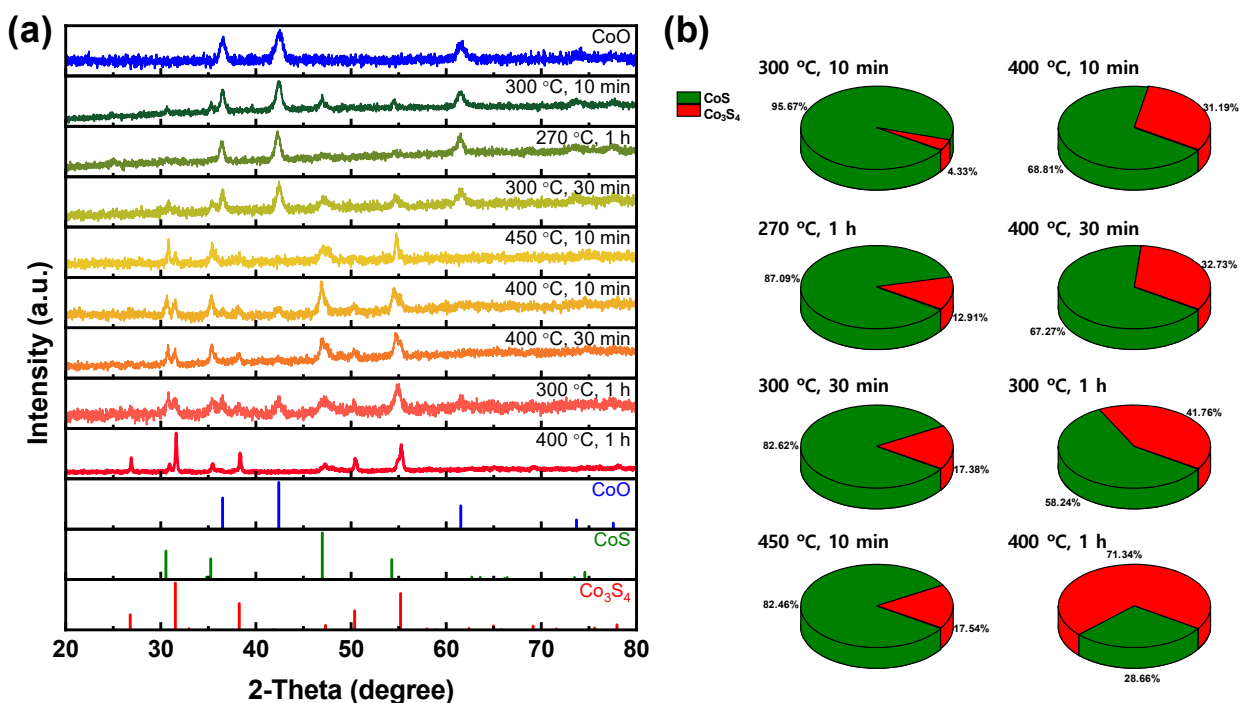


**Fig. S10** (a) XRD patterns of CoO/CoS<sub>x</sub> obtained at various reaction conditions and (b) CoS and Co<sub>3</sub>S<sub>4</sub> composition ratios determined by Rietveld refinement.

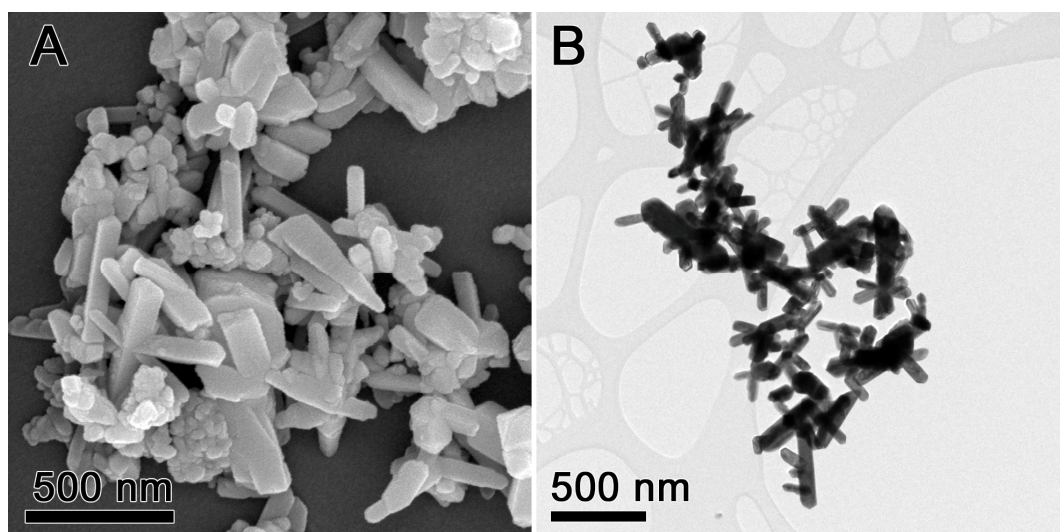


**Fig. S11** (a) SEM and (b) TEM images of commercially available  $\text{IrO}_2$ .

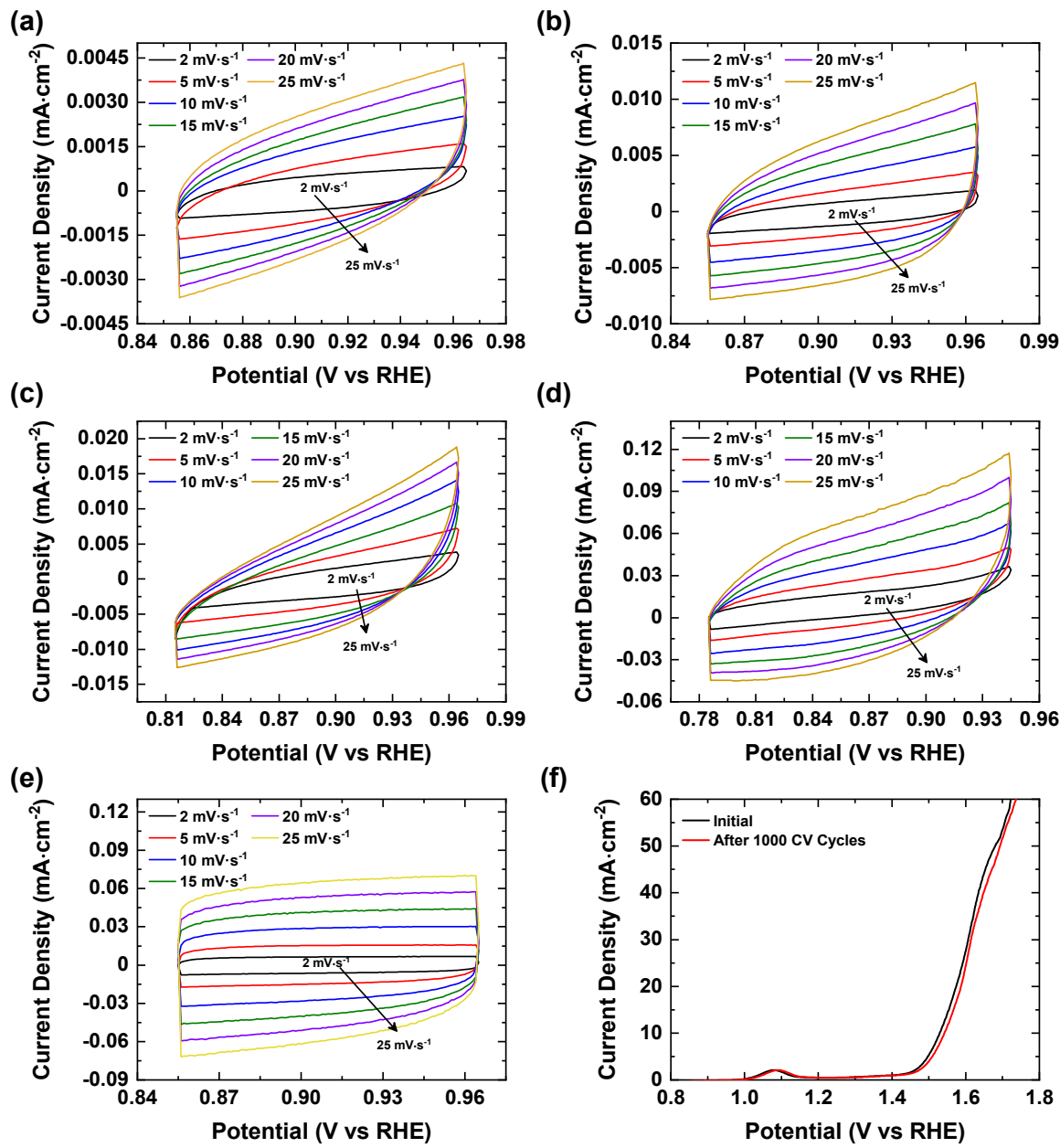


**Fig. S12** Cyclic voltammograms of (a) Bare GC, (b)  $\text{Co}_3\text{O}_4$ , (c) CoO, (d)  $\text{CoO}/\text{CoS}_x$ , and (e)  $\text{IrO}_2$  electrodes in 0.1 M KOH at various scan rates to determine the electrochemical double layer capacitance ( $C_{dl}$ ). (f) Linear scan voltammograms of  $\text{CoO}/\text{CoS}_x$  as an electrocatalyst for OER before and after 1000 CV scans, demonstrating excellent stability of  $\text{CoO}/\text{CoS}_x$ .

**Table S3** The ECSA calculations of each catalyst.

Sample	Slope ( $\text{mF}\cdot\text{cm}^{-2}$ )	$C_{dl}$ ( $\text{mF}\cdot\text{cm}^{-2}$ )	$R_f$	ECSA ( $\text{cm}^2$ )
Bare GC	0.154	0.077	-	-
$\text{CO}_3\text{O}_4$	0.427	0.214	2.77	0.54
CoO	0.458	0.229	2.98	0.58
$\text{CoO}/\text{CoS}_x$	3.7	1.85	23.99	4.70
$\text{IrO}_2$	4.85	2.425	31.45	6.16

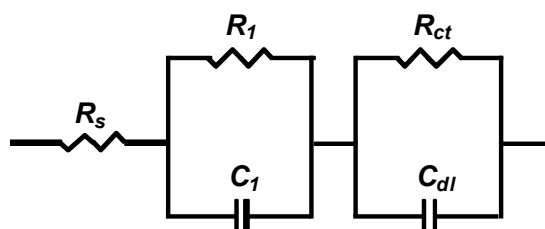


**Fig. S13** Equivalent circuit used for fitting the impedance spectra of OER electrocatalysts.  $R_s$  represents the solution resistance.  $R_1$  and  $C_1$  denote the diffusion/adsorption of reaction intermediates due to slow diffusion through the reaction interface in the porous electrode.  $R_2$  and  $C_{dl}$  are ascribed to the charge transfer resistance the capacitance associated with OER, respectively.

**Table S4** Various resistance values extracted by fitting the equivalent circuit in Fig. S5 to the Nyquist plots of various cobalt oxides and  $\text{IrO}_2$  when employed as OER electrocatalysts.

Catalyst	$R_s$ ( $\Omega\cdot\text{cm}^2$ )	$R_1$ ( $\Omega\cdot\text{cm}^2$ )	$R_{ct}$ ( $\Omega\cdot\text{cm}^2$ )
$\text{CO}_3\text{O}_4$	2.30	111.82	952.36
CoO	1.19	0.97	185.24
$\text{CoO}/\text{CoS}_x$	1.87	0.38	21.77
$\text{IrO}_2$	2.11	1.77	40.68

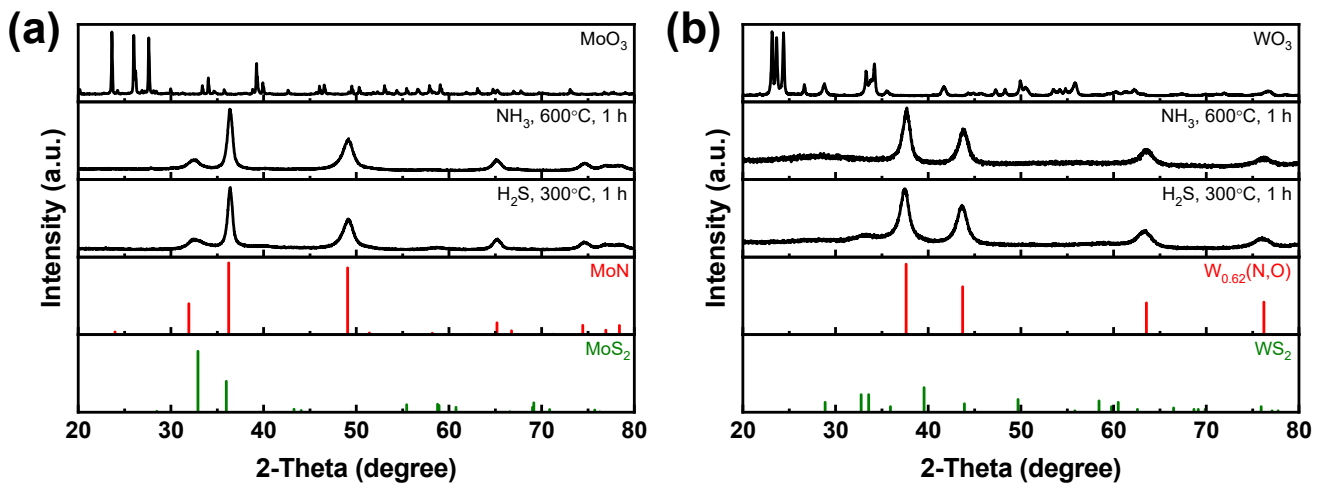


**Fig. S14** XRD patterns taken during the synthesis of (a) nanostructured MoN/MoS<sub>2</sub> and (b) nanostructured W<sub>0.62</sub>(N,O)/WS<sub>2</sub>.

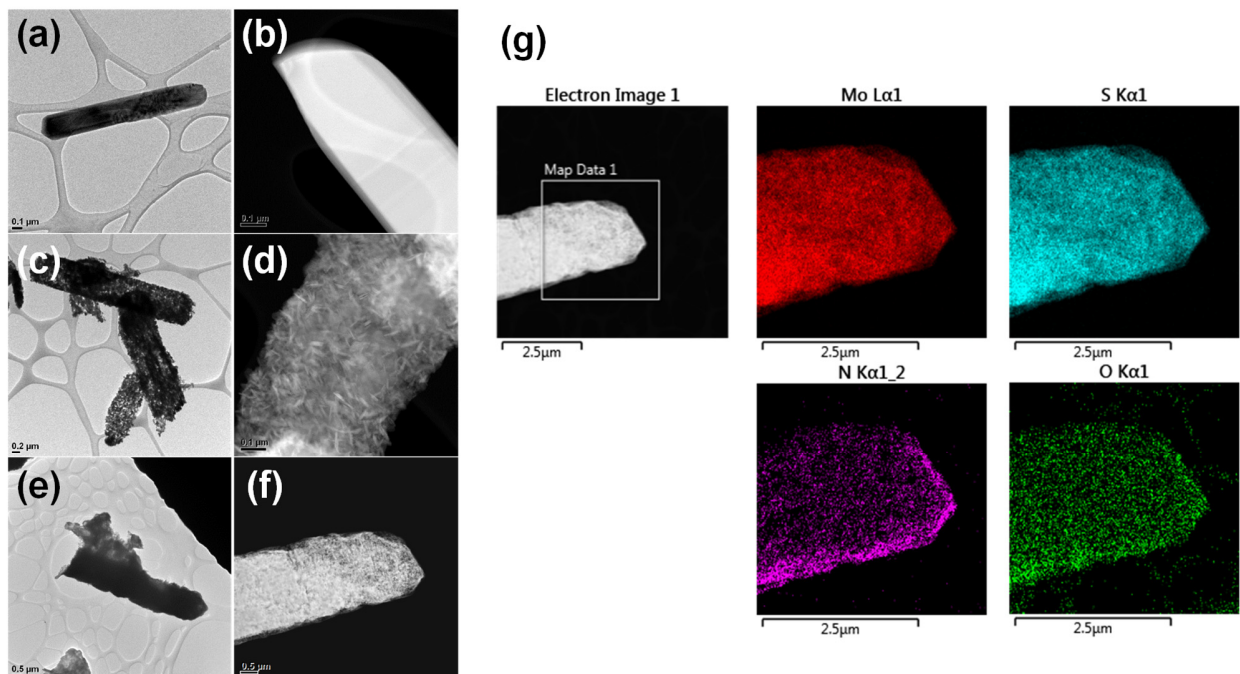


**Fig. S15** TEM images of taken during the synthesis of nanostructured MoN/MoS<sub>2</sub>: (a,b) MoO<sub>3</sub>, (c,d) MoN, (e,f) MoN/MoS<sub>2</sub>, and (g) STEM-EDS mapping analysis results of MoN/MoS<sub>2</sub>.

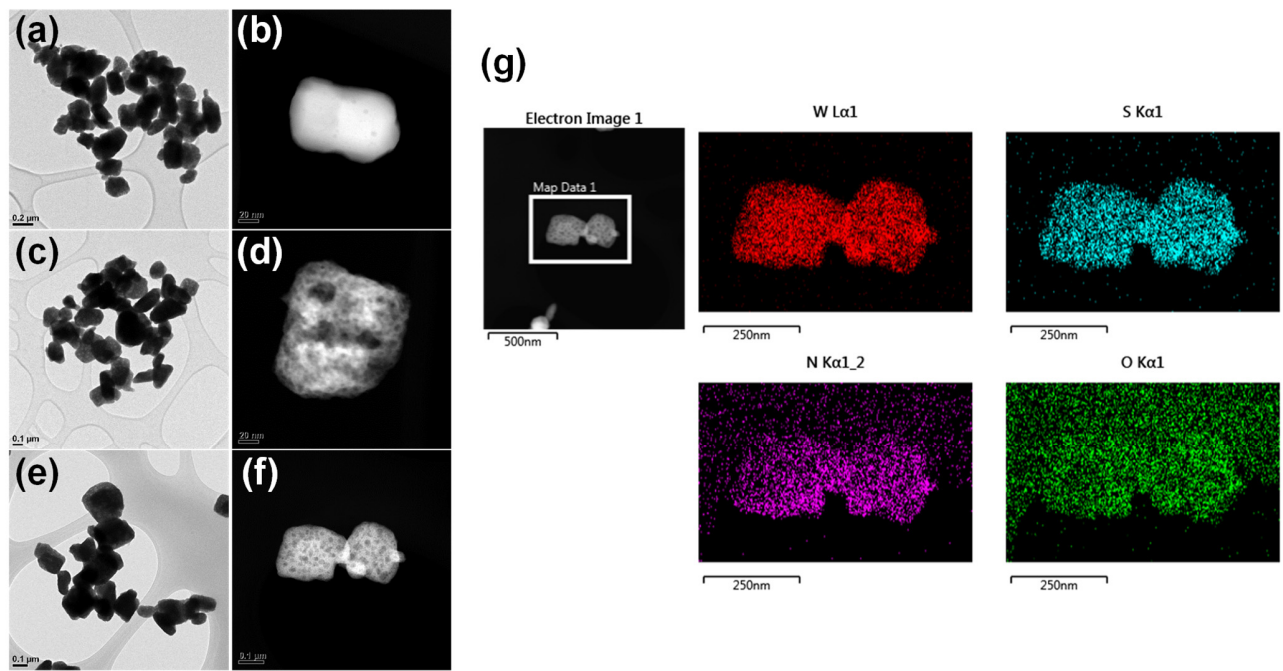


**Fig. S16** TEM images of taken during the synthesis of nanostructured  $\text{W}_{0.62}(\text{N},\text{O})/\text{WS}_2$ : (a,b)  $\text{WO}_3$ , (c,d)  $\text{W}_{0.62}(\text{N},\text{O})$ , (e,f)  $\text{W}_{0.62}(\text{N},\text{O})/\text{WS}_2$ , and (g) STEM-EDS mapping analysis results of  $\text{W}_{0.62}(\text{N},\text{O})/\text{WS}_2$ .